IEEE Access
Multidisciplinary | Rapid Review | Open Access Journal

Received April 28, 2018, accepted May 28, 2018, date of publication June 1, 2018, date of current version June 29, 2018.

Digital Object Identifier 10.1109/ACCESS.2018.2842747

Impact Dynamics Prediction of a Rotary-Percussive Ultrasonic Drill With a Free Mass

DEEN BAI, (Student Member, IEEE), QIQUAN QUAN, (Member, IEEE), YINCHAO WANG, HE LI, PENGYUE ZHAO, AND ZONGQUAN DENG

State Key Laboratory of Robotics and System, Harbin Institute of Technology, Harbin 150001, China

Corresponding author: Qiquan Quan (quanqiquan@hit.edu.cn)

This work was supported in part by the National Natural Science Foundation of China under Grant 61403106, in part by the Program of Introducing Talents of Discipline to Universities under Grant B07018, and in part by the National Natural Science Foundation of China under Grant 51521003.

ABSTRACT The rotary-percussive ultrasonic drill (RPUD) employs vibrations on two sides of a piezoelectric stack to drive a drill tool to achieve simultaneous rotary-percussive motion. It has the advantages of being small and requiring low power, low axial load, and small holding torque, making it suitable for extra-terrestrial rock sampling, especially for a minor planet with a weak gravitational field. This paper presents the impact dynamics prediction of the percussive system of RPUD, which is composed of a piezoelectric actuator, a free mass, and a drill tool. Considering the vibration of the RPUD and the weight on bit, the interactions between these three components before and during drilling are analyzed separately. The effects of various parameters (i.e., the coefficient of restitution between the actuator and the free mass, the damping ratio of the RPUD, the weight of the free mass, and the weight on bit) on the contact force between the free mass and the drill tool, a number of collisions per second, kinetic energy transferred to the drill tool per second, and reacting force are simulated. Simulation results show that the free mass converts the high-frequency harmonic vibration of the actuator into lower frequency impacts on the drill tool. Furthermore, the contact force and the kinetic energy transferred to the drill tool per second can be enhanced by increasing the coefficient of restitution, free mass, and weight on bit or decreasing the damping ratio of the RPUD.

INDEX TERMS Planetary exploration, ultrasonic drill, rotary-percussive ultrasonic drill, piezoelectric actuator, impact dynamics.

I. INTRODUCTION

Obtaining lunar regolith and soil/rock samples of other planetary bodies is vital to the study and understanding of the environment on the moon and other planetary bodies with the ultimate goal of facilitating human colonization [1]. In planetary exploration missions to obtain soil/rock samples, drilling is often the method of choice [2], [3]. However, the challenges facing conventional drilling devices driven by electromagnetic motors are the large axial forces and holding torques needed, which means that a probe should have a relatively large mass. To address these challenges, a percussive ultrasonic/sonic driller/corer (USDC) that employs the high frequency longitudinal vibration of a piezoelectric actuator to fracture rocks was developed [4], [5]. Compared with conventional drilling devices, the USDC has the advantages of having a small size, low power, low axial force, and small holding torque [6]–[11].

Piezoelectric actuators have been widely used in applications such as robot joints, high-precision machines, micro-robots, nanopositioning stages, and microelectromechanical systems [12]–[15]. Based on the structure, piezoelectric actuators can be classified into bonded type actuators [16]–[19] and bolt-clamped type actuators [20], [21]. Bolt-clamped type actuators usually clamp the lead zirconate titanate (PZT) elements between metal blocks with a bolt. A larger preload can be applied on the PZT elements without fatigue of the adhesive layer. Therefore, higher excitation voltage can be applied to achieve a larger output power than with the bonded type [22]–[24]. Furthermore, compared with the bonded type actuators that adopt a d_{31} working mode in which the stress

and poling directions of the PZT elements are perpendicular, the bolt-clamped type actuators adopt a d_{33} working mode, in which the stress and poling directions of the PZT elements coincide, and provide greater output power and efficiency [25].

The USDC is composed of three main components: a bolt-clamped type actuator, a free mass, and a drill tool. The harmonic vibration of the bottom side of the ultrasonic actuator drives the free mass to oscillate between the actuator and the drill tool. The free mass impacts the drill tool, creating a stress wave which propagates through the drill tool and is transferred to the interface between the rock and the drill tool. Once the stress exceeds the ultimate strain of the rock, it will crack [26]–[28].

To remove the cuttings generated at the bottom of the hole and increase the efficiency of the USDC during drilling, rotary-percussive ultrasonic drills (RPUDs) that utilizing a piezoelectric actuator to realize the rotary and percussive motion of the drill tool are proposed [29], [30]. The piezoelectric actuator for the RPUD is a type of bolt-clamped type actuator with a piezoelectric stack being clamped between a stepped horn and a longitudinal-torsional coupler. The bottom side of the actuator generates high-frequency harmonic vibration while the upper side outputs elliptical trajectories which drives the drill tool to rotate via a transmission system. The RPUD is mounted on the end of the manipulator of the probe and acts as an end effector. When drilling rocks on the planetary bodies with weak gravitational field, the weight on bit applied on the RPUD, which is usually provided by the gravity of the probe, is constrained. Furthermore, the vibration of the RPUD leads to fluctuations in the reacting force acting on the probe. To date, the impact dynamics analyses of the RPUD have not considered the effect of the weight on bit or the reacting force acting on the probe.

Considering the vibration of the RPUD and the weight on bit, the impact dynamics prediction for the percussive system of the RPUD before and during drilling a rock is discussed in this paper. Before drilling a rock, an exciting voltage is applied to the actuator, and the drill tool does not make contact with the rock. The effect of the rotary motion of the drill tool on the percussive system is ignored. The motion of the RPUD after collision with the free mass is modeled as an equivalent generalized single-degree-of-freedom (SDOF) system. Then, the vibration equation of the bottom side of the actuator includes the harmonic vibration of the actuator excited by the sinusoidal voltage and the free vibration of the SDOF system. The velocities of the actuator and the free mass after collision are calculated by applying the principle of conservation of momentum. After collision with the actuator, the movement of the free mass is assumed to be free-falling, therein ignoring the frictional force. The motion of the drill tool is also modeled as a SDOF system, of which the initial velocity can be obtained by applying the principle of conservation of momentum. The position of each component of the percussive mechanism as a function of time is calculated by a computer code. During drilling into a rock, the collision process between the actuator and the free mass is the same as the process before drilling. Considering that the drill tool is inserted into the drill hole, the bottom side of the drill tool is assumed to be fixed. The collision between the free mass and the drill tool is analysed using the energy balance method.

The remainder of this paper is organized as follows. In Section II, the structure and operating principle of the RPUD are presented. Collisions between the actuator, the free mass, and the drill tool before drilling are analysed and simulated by a computer code in Section III. In Section IV, the impact dynamics prediction for the percussive system during drilling is presented, simulated, and discussed. Finally, the conclusions are drawn in Section V.

II. STRUCTURE AND OPERATING PRINCIPLE OF THE RPUD

The RPUD utilizes one bolt-clamped type longitudinal and longitudinal-torsional (L-LT) actuator to realize the rotary and percussive motion of the drill tool. The configuration of the L-LT actuator and the RPUD are shown in Fig. 1. The L-LT actuator is composed of a stepped horn, a longitudinal-torsional (LT) coupler, four PZT ceramic rings, and five electrodes. The polarization directions of the adjacent PZT ceramic rings that are polarized along their thickness directions are opposite and are marked with "+" and "−", as shown in Fig. 1(a). The four ceramic rings and five electrodes constitute one piezoelectric stack which is clamped between the stepped horn and the LT coupler. Excited by a sinusoidal voltage of which the frequency is equal to the

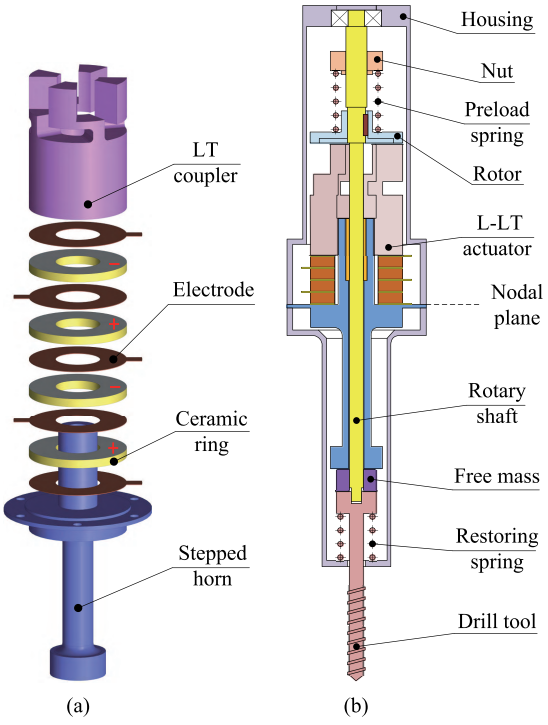

FIGURE 1. Configuration of the RPUD and the L-LT actuator. (a) The exploded diagram of the L-LT actuator. (b) The configuration of the RPUD.

resonance frequency of the L-LT actuator, the piezoelectric stack generates longitudinal vibration along its axial direction on both sides. Then, the stepped horn enlarges the longitudinal vibrations of the bottom side of the piezoelectric stack and generates high-frequency harmonic vibrations at the bottom of the actuator. Meanwhile, the LT coupler converts the longitudinal vibration of the upper side of the piezoelectric stack into longitudinal-torsional vibration and forms elliptical trajectories at the end of the LT coupler. Fig. 1(b) shows the configuration of the RPUD. The bottom of the actuator impacts the free mass and drives it to move toward the drill tool. Then, the free mass collides with the drill tool to generate a stress wave which propagates along the drill tool. The elliptical trajectories at the upper side of the actuator push the rotor into rotary motion using the frictional force provided by the preload spring. Finally, the rotor drives the drill tool to rotate via a rotary shaft.

III. INTERACTION OF THE PERCUSSIVE MECHANISM COMPONENTS BEFORE ROCK DRILLING

This section focuses on studying the impact dynamics of the percussive system before the drill tool contacts the rock with the actuator being excited by a sinusoidal voltage. The collision model of the RPUD before rock drilling is shown in Fig. 2. The RPUD is mounted on a linear guide which connects to the body frame of the probe, as shown in Fig. 2(a); the two ends of the load spring connect to the RPUD and the load unit separately. The drill tool is not in contact with the rock. The free mass collides with the actuator and the drill tool alternately, as shown in Fig. 2(b). Some assumptions should be made before establishing the collision model.

1) The nodal plane of the actuator is located on the bottom side of the piezoelectric stack.
2) The motion of the bottom side of the actuator is a simple harmonic vibration.
3) The harmonic vibration process is not affected by the collision with the free mass.
4) The drill tool is not in contact with the rock and can vibrate freely along the axial direction.
5) When the free mass oscillates between the drill tool and the actuator, the friction force between the free mass and the rotary shaft is ignored.
6) The rotary motion of the drill tool has no effect on the percussive system.

A. COLLISION BETWEEN THE ACTUATOR AND THE FREE MASS

The displacement, $u_{\mathrm{hv}}(t)$, and velocity, $v_{\mathrm{hv}}(t)$, for the harmonic vibration of the bottom side of the actuator, which is excited by a sinusoidal voltage, as functions of time, t, are given by

$$\begin{cases} u_{\mathrm{hv}}(t) = A_0 \sin(2\pi f_0 t) \\ v_{\mathrm{hv}}(t) = 2\pi f_0 A_0 \cos(2\pi f_0 t) \end{cases} \tag{1}$$

where A_0 and f_0 is the amplitude and the frequency of the harmonic vibration, separately.

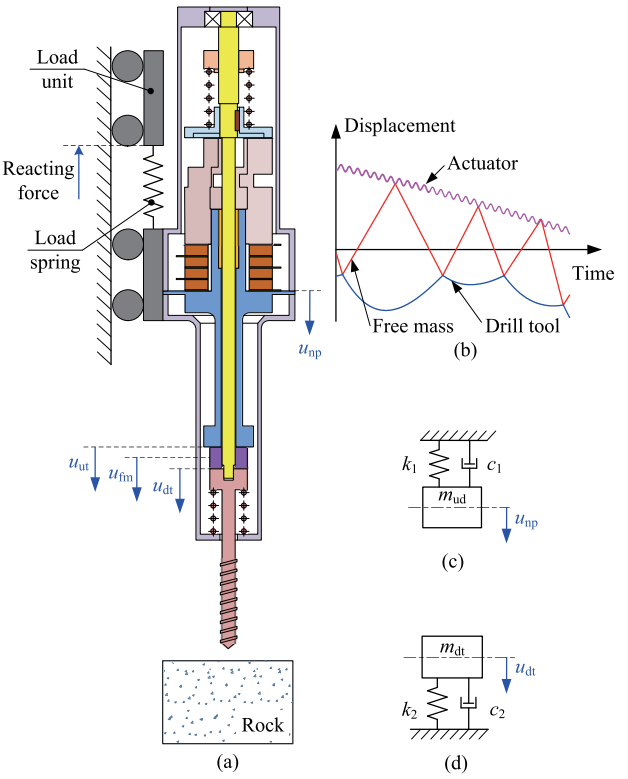

FIGURE 2. Collision model of the RPUD before drilling. (a) The composition of collision system. (b) The position of each component as a function of time. (c) The equivalent SDOF system for the RPUD. (d) The equivalent SDOF system for the free mass and the drill tool.

After collision with the free mass, the remaining parts of the RPUD, except for the free mass and the drill tool, will move up and down along the guide. Considering that the mounting surface of the actuator coincides with the nodal plane, the displacement of the nodal plane is regarded as the displacement of the RPUD. The movement of the RPUD, which is supported by the load spring, is modeled as an SDOF system, as shown in Fig. 2(c). The equation of motion for the nodal plane of the actuator is given by

$$m_{\mathrm{ud}}\ddot{u}_{\mathrm{np}}(t) + c_1\dot{u}_{\mathrm{np}}(t) + k_1 u_{\mathrm{np}}(t) = 0 \tag{2}$$

where $u_{\mathrm{np}}(t)$ is the displacement of the nodal plane as a function of time, m_{ud} is the mass of the RPUD, $c_1 = 2\xi_{\mathrm{ud}}\omega_{\mathrm{nud}}m_{\mathrm{ud}}$ is the damping coefficient, ξ_{ud} is the damping ratio, $\omega_{\mathrm{nut}} = \sqrt{k_1/m_{\mathrm{ud}}}$ is the natural frequency of the SDOF system, and k_1 is the spring rate of the load spring. Considering the motion of the nodal plane and the harmonic vibration excited by the sinusoidal voltage, the absolute displacement, $u_{\mathrm{ut}}(t)$, and the absolute velocity, $v_{\mathrm{ut}}(t)$, of the bottom side of the actuator are given by

$$\begin{cases} u_{\mathrm{ut}}(t) = u_{\mathrm{np}}(t) + u_{\mathrm{hv}}(t) \\ v_{\mathrm{ut}}(t) = v_{\mathrm{np}}(t) + v_{\mathrm{hv}}(t) \end{cases} \tag{3}$$

In the following sections, the absolute displacement of the bottom side of the actuator is called the displacement of the actuator for short. In addition, the absolute velocity of

the bottom side of the actuator is called the velocity of the actuator for short. Assuming that the actuator impacts the free mass at time t_m, the velocities of the actuator and the free mass before and after the collision follow the law of conservation of momentum, as in

$$m_{\mathrm{ud}}v_{\mathrm{ut}}(t_m) + m_{\mathrm{fm}}v_{\mathrm{fm}}(t_m) = m_{\mathrm{ud}}v'_{\mathrm{ut}}(t_m) + m_{\mathrm{fm}}v'_{\mathrm{fm}}(t_m) \quad (4)$$

where m_{fm} is the mass of the free mass, $v_{\mathrm{fm}}(t_m)$ and $v'_{\mathrm{fm}}(t_m)$ are the velocity of the free mass immediately before and after the collision, respectively, and $v'_{\mathrm{ut}}(t_m)$ is the velocity of the actuator immediately after impact.

The coefficient of restitution for the collision between the actuator and the free mass, e_1, is given by

$$e_1 = \frac{v'_{\mathrm{ut}}(t_m) - v'_{\mathrm{fm}}(t_m)}{v_{\mathrm{fm}}(t_m) - v_{\mathrm{ut}}(t_m)} \quad (5)$$

Then, using (4) and (5), the velocities of the actuator and the free mass after collision are given by

$$\begin{cases} v'_{\mathrm{fm}}(t_m) = \dfrac{m_{\mathrm{fm}} - e_1 m_{\mathrm{ud}}}{m_{\mathrm{ud}} + m_{\mathrm{fm}}} v_{\mathrm{fm}}(t_m) \\ \qquad\qquad + \dfrac{(1+e_1)\, m_{\mathrm{ud}}}{m_{\mathrm{ud}} + m_{\mathrm{fm}}} v_{\mathrm{ut}}(t_m) \\ v'_{\mathrm{ut}}(t_m) = \dfrac{m_{\mathrm{ud}} - e_1 m_{\mathrm{fm}}}{m_{\mathrm{ud}} + m_{\mathrm{fm}}} v_{\mathrm{ut}}(t_m) \\ \qquad\qquad + \dfrac{(1+e_1)\, m_{\mathrm{fm}}}{m_{\mathrm{ud}} + m_{\mathrm{fm}}} v_{\mathrm{fm}}(t_m) \end{cases} \quad (6)$$

The displacement, $u'_{\mathrm{np}}(t_m)$, and velocity, $v'_{\mathrm{np}}(t_m)$, of the nodal plane after collision immediately are given by

$$\begin{cases} u'_{\mathrm{np}}(t_m) = u_{\mathrm{np}}(t_m) \\ v'_{\mathrm{np}}(t_m) = v'_{\mathrm{ut}}(t_m) - v_{\mathrm{hv}}(t_m) \end{cases} \quad (7)$$

The dynamic response of the RPUD after collision is obtained by using the position and velocity of the nodal plane after impact as initial conditions for the SDOF system of the RPUD. Therefore, the free vibration response of the nodal plane is given by

$$\begin{cases} u_{\mathrm{np}}(t) = e^{-a_{\mathrm{ud}}(t-t_m)} \{ \mathrm{A}_1 \cos[\omega_{\mathrm{dud}}(t-t_m)] \\ \qquad + \mathrm{A}_2 \sin[\omega_{\mathrm{dud}}(t-t_m)] \} \\ v_{\mathrm{np}}(t) = -a_{\mathrm{ud}} e^{-a_{\mathrm{ud}}(t-t_m)} \{ \mathrm{A}_1 \cos[\omega_{\mathrm{dud}}(t-t_m)] \\ \qquad + \mathrm{A}_2 \sin[\omega_{\mathrm{dud}}(t-t_m)] \} \\ \qquad + \omega_{\mathrm{dud}} e^{-a_{\mathrm{ud}}(t-t_m)} \{ -\mathrm{A}_1 \sin[\omega_{\mathrm{dud}}(t-t_m)] \\ \qquad + \mathrm{A}_2 \cos[\omega_{\mathrm{dud}}(t-t_m)] \} \end{cases} \quad (8)$$

where $\omega_{\mathrm{dud}} = \omega_{\mathrm{nud}}\sqrt{1-\xi_{\mathrm{ud}}^2}$ is the damped natural frequency of the RPUD, $a_{\mathrm{ud}} = \xi_{\mathrm{ud}}\omega_{\mathrm{nud}}$ is a coefficient relating to the SDOF system of the RPUD, and A_1 and A_2 are undetermined coefficients, as in

$$\begin{cases} \mathrm{A}_1 = u'_{\mathrm{np}}(t_m) \\ \mathrm{A}_2 = \dfrac{v'_{\mathrm{np}}(t_m) + \xi_{\mathrm{ud}}\omega_{\mathrm{nud}} u'_{\mathrm{np}}(t_m)}{\omega_{\mathrm{dud}}} \end{cases} \quad (9)$$

Then, the displacement, $u_{\mathrm{ut}}(t)$, and velocity, $v_{\mathrm{ut}}(t)$, of the actuator as functions of time before the next collision can be calculated using (1), (3), and (8). The displacement, $u_{\mathrm{fm}}(t)$, and velocity, $v_{\mathrm{fm}}(t)$, of the free mass before the next collision are given by

$$\begin{cases} u_{\mathrm{fm}}(t) = u'_{\mathrm{fm}}(t_m) + v'_{\mathrm{fm}}(t_m)(t-t_m) + \frac{1}{2}g(t-t_m)^2 \\ v_{\mathrm{fm}}(t) = v'_{\mathrm{fm}}(t_m) + g(t-t_m) \end{cases} \quad (10)$$

where $u'_{\mathrm{fm}}(t_m) = u_{\mathrm{fm}}(t_m)$ is the displacement of the free mass immediately after the collision and g is the acceleration of gravity.

B. COLLISION BETWEEN THE FREE MASS AND THE DRILL TOOL

After collision with the actuator, the free mass moves toward the drill tool. Assuming that the free mass impacts the drill tool at time t_n, the velocities of the free mass and the drill tool before and after the collision follow the law of conservation of momentum, as in

$$m_{\mathrm{fm}}v_{\mathrm{fm}}(t_n) + m_{\mathrm{dt}}v_{\mathrm{dt}}(t_n) = m_{\mathrm{fm}}v'_{\mathrm{fm}}(t_n) + m_{\mathrm{dt}}v'_{\mathrm{dt}}(t_n) \quad (11)$$

where $v(t_n)$ is the velocity immediately before impact at time t_n, $v'(t_n)$ is the velocity immediately after impact, and the subscripts fm and dt correspond to the free mass and the drill tool, respectively. Furthermore, m_{dt} is the mass of the drill tool. The coefficient of restitution for the collision between the free mass and the drill tool, e_2, is given by

$$e_2 = \frac{v'_{\mathrm{fm}}(t_n) - v'_{\mathrm{dt}}(t_n)}{v_{\mathrm{dt}}(t_n) - v_{\mathrm{fm}}(t_n)} \quad (12)$$

Then, using (11) and (12), the velocities of the free mass, v'_{fm}, and the drill tool, v'_{dt}, after collision are given by

$$\begin{cases} v'_{\mathrm{dt}}(t_n) = \dfrac{m_{\mathrm{dt}} - e_2 m_{\mathrm{fm}}}{m_{\mathrm{fm}} + m_{\mathrm{dt}}} v_{\mathrm{dt}}(t_n) \\ \qquad\qquad + \dfrac{(1+e_2)\, m_{\mathrm{fm}}}{m_{\mathrm{fm}} + m_{\mathrm{dt}}} v_{\mathrm{fm}}(t_n) \\ v'_{\mathrm{fm}}(t_n) = \dfrac{m_{\mathrm{fm}} - e_2 m_{\mathrm{dt}}}{m_{\mathrm{fm}} + m_{\mathrm{dt}}} v_{\mathrm{fm}}(t_n) \\ \qquad\qquad + \dfrac{(1+e_2)\, m_{\mathrm{dt}}}{m_{\mathrm{fm}} + m_{\mathrm{dt}}} v_{\mathrm{dt}}(t_n) \end{cases} \quad (13)$$

After colliding with the free mass, the drill tool, which is supported by the restoring spring, moves up and down along its axial direction. The movement of the drill tool is modeled as a SDOF system, as shown in Fig. 2(d). The equation of motion for the SDOF system of the drill tool is given by

$$m_{\mathrm{dt}}\ddot{u}_{\mathrm{dt}}(t) + c_2\dot{u}_{\mathrm{dt}}(t) + k_2 u_{\mathrm{dt}}(t) = 0 \quad (14)$$

where $u_{\mathrm{dt}}(t)$ is the displacement of the drill tool as a function of time, $c_2 = 2\xi_{\mathrm{dt}}\omega_{\mathrm{ndt}}m_{\mathrm{dt}}$ is the damping coefficient of the drill tool, ξ_{dt} is the damping ratio, $\omega_{\mathrm{ndt}} = \sqrt{k_2/m_{\mathrm{dt}}}$ is the natural frequency of the SDOF system of the drill tool, and k_2 is the spring rate of the restoring spring.

The dynamic response of the drill tool after collision is obtained using the position and velocity of the drill tool

immediately after impact as initial conditions. The free vibration response of the drill tool is given by

$$\begin{cases} u_{\mathrm{dt}}(t) = e^{-a_{\mathrm{dt}}(t-t_n)}\{B_1\cos[\omega_{\mathrm{ddt}}(t-t_n)] \\ \qquad + B_2\sin[\omega_{\mathrm{ddt}}(t-t_n)]\} \\ v_{\mathrm{dt}}(t) = -a_{\mathrm{dt}}e^{-a_{\mathrm{dt}}(t-t_n)}\{B_1\cos[\omega_{\mathrm{ddt}}(t-t_n)] \\ \qquad + B_2\sin[\omega_{\mathrm{ddt}}(t-t_n)]\} \\ +\omega_{\mathrm{ddt}}e^{-a_{\mathrm{dt}}(t-t_n)}\{-B_1\sin[\omega_{\mathrm{ddt}}(t-t_n)] \\ \qquad + B_2\cos[\omega_{\mathrm{ddt}}(t-t_n)]\} \end{cases} \tag{15}$$

where $\omega_{\mathrm{ddt}} = \omega_{\mathrm{ndt}}\sqrt{1-\xi_{\mathrm{dt}}^2}$ is the damped natural frequency of the SDOF system of the drill tool, and $a_{\mathrm{dt}} = \xi_{\mathrm{dt}}\omega_{\mathrm{ndt}}$ is a coefficient relating to the SDOF system of the drill tool. B_1 and B_2 are undetermined coefficients and are given by

$$\begin{cases} B_1 = u'_{\mathrm{dt}}(t_n) \\ B_2 = \dfrac{v'_{\mathrm{dt}}(t_n) + \xi_{\mathrm{dt}}\omega_{\mathrm{ndt}}u'_{\mathrm{dt}}(t_n)}{\omega_{\mathrm{ddt}}} \end{cases} \tag{16}$$

Then, the displacement, $u_{\mathrm{ut}}(t)$, and velocity, $v_{\mathrm{ut}}(t)$, of the drill tool before the next collision as functions of time can be calculated using (15) and (16). The displacement, $u_{\mathrm{fm}}(t)$, and velocity, $v_{\mathrm{fm}}(t)$, of the free mass after the collision with the drill tool are given by

$$\begin{cases} u_{\mathrm{fm}}(t) = u'_{\mathrm{fm}}(t_n) + v'_{\mathrm{fm}}(t_n)(t-t_n) + \frac{1}{2}g(t-t_n)^2 \\ v_{\mathrm{fm}}(t) = v'_{\mathrm{fm}}(t_n) + g(t-t_n) \end{cases} \tag{17}$$

where $u'_{\mathrm{fm}}(t_n) = u_{\mathrm{fm}}(t_n)$ is the displacement of the free mass at the time t_n.

C. SIMULATION AND DISCUSSION

To obtain a visual understanding of the collision process, a computer code is developed to analyze the collision model of the actuator, the free mass, and the drill tool before drilling. The initial parameters of the collision system are given in Table 1. The collision process through the time between the actuator, the free mass, and the drill tool is obtained through calculation. Assume the coefficient of restitution, e_1 and e_2, are both equal to one, and the damping ratio, ξ_{ud} and ξ_{dt}, are both equal to 0.5.

TABLE 1. Simulation parameters for the percussive system before rock drilling.

Simulation parameter	Value
Mass of the RPUD m_{ud}	1000 g
Frequency of harmonic vibration f_0	16000 Hz
Amplitude of harmonic vibration A_0	35 μm
Damping ratio of the RPUD ξ_{ud}	0.5
Spring rate of the load spring k_1	2000 N/m
Mass of the free mass m_{fm}	5 g
Mass of the drill tool m_{dt}	13.5 g
Damping ratio of the drill tool ξ_{dt}	0.5
Spring rate of the restoring spring k_2	2000 N/m
Coefficient of restitution e_1	1
Coefficient of restitution e_2	1

The displacements of the actuator, the free mass, and the drill tool as functions of time in the initial 0.6 seconds are shown in Fig. 3. The simulation results indicate that the free mass, which oscillates between the actuator and the drill tool, impacts the drill tool approximately 260 times in 0.6 seconds, meaning that the impact frequency of the drill tool is nearly 430 Hz. Fig. 4 shows a local zoomed in graph of the Fig. 3. In each oscillation cycle of the free mass, the end tip of the actuator experiences several cycles, which indicates that the free mass converts the high frequency and small amplitude harmonic vibration of the actuator into lower frequency and large amplitude impacts on the drill tool. Fig. 5 gives the curve of the reacting force acting on the load unit as a function of time in the initial 5 seconds. It is observed that the average value of the reacting force is 5.8 N.

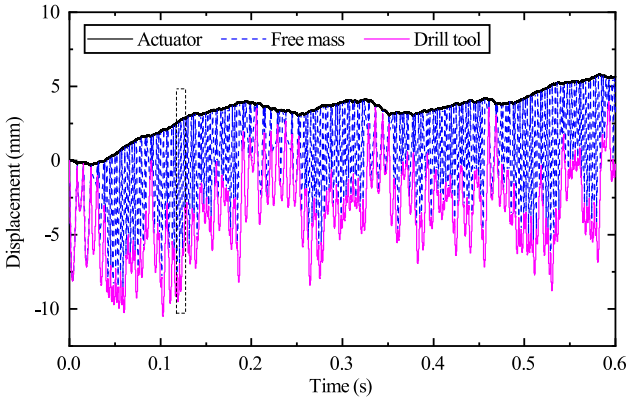

FIGURE 3. Positions of the actuator, the free mass and the drill tool as functions of time before rock drilling.

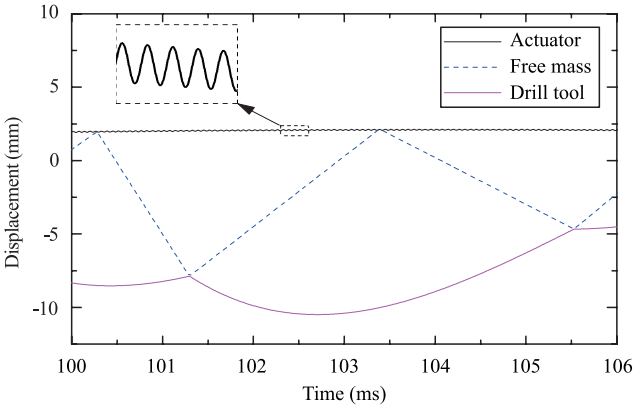

FIGURE 4. Local zoomed in graph of Fig. 3. showing positions of the actuator, the free mass and the drill tool.

IV. INTERACTION OF THE PERCUSSIVE MECHANISM COMPONENTS DURING ROCK DRILLING

This section focuses on studying the impact dynamics of the percussive system during rock drilling. Collision model of the RPUD before drilling is shown in Fig. 6. During rock drilling, the RPUD moves along the guide; the weight on bit is applied by a load spring, of which compression can be adjusted by the load unit. The bottom end of the drill tool

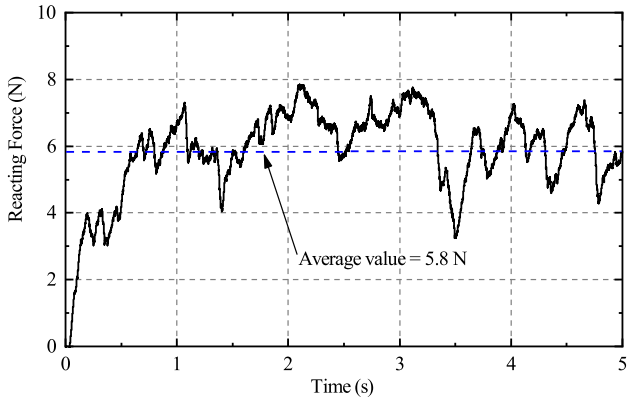

FIGURE 5. Reacting force acting on the load unit versus time before rock drilling.

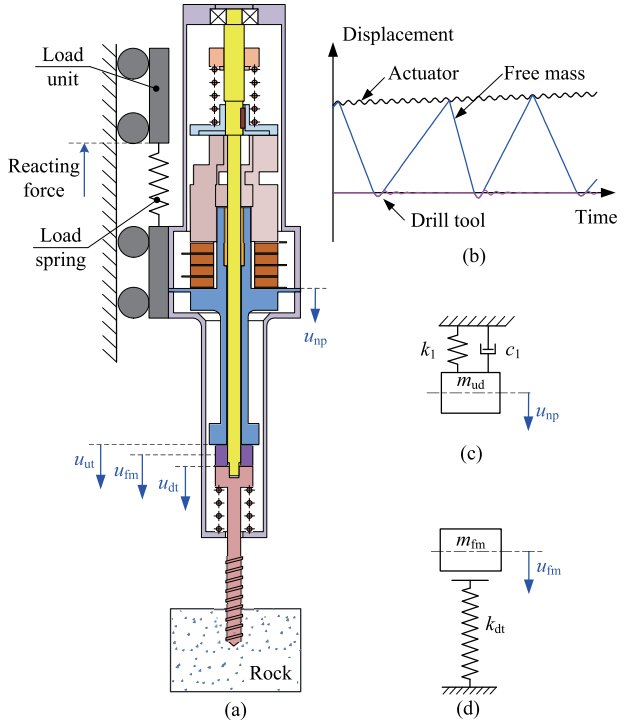

FIGURE 6. Collision model of the RPUD during rock drilling. (a) The composition of collision system. (b) The position of each component as a function of time. (c) The equivalent SDOF system for the RPUD. (d) The equivalent spring system for the free mass and the drill tool.

is inserted into the drill hole, as show in Fig. 6(a). The free mass collides with the actuator and the drill tool alternately and oscillates between them, as shown in Fig. 6(b). Some assumptions have been made before establishing the collision model.

1) The nodal plane of the actuator is located on the bottom side of the piezoelectric stack.
2) The motion of the bottom side of the actuator is a simple harmonic vibration.
3) The harmonic vibration process is not affected by the collision with the free mass.
4) The bottom side of the drill tool is fixed.
5) When the free mass oscillates between the drill tool and the actuator, the friction force between the free mass and the rotary shaft is ignored.
6) The rotary motion of the drill tool has no effect on the percussive system.

A. COLLISION BETWEEN THE ACTUATOR AND THE FREE MASS

The collision process of the actuator and the free mass during rock drilling is similar to the process before rock drilling presented in Section III. According to (1), (3), (8), and (9), the displacement, $u_{\mathrm{ut}}(t)$, and velocity, $v_{\mathrm{ut}}(t)$, of the actuator after t_i when the actuator and the free mass occurs on the ith collision are given by

$$\begin{cases} u_{\mathrm{hv}}(t) = A_0 \sin(2\pi f_0 t) \\ v_{\mathrm{hv}}(t) = 2\pi f_0 A_0 \cos(2\pi f_0 t) \\ u_{\mathrm{np}}(t) = e^{-a_{\mathrm{ud}}(t-t_i)}\{\mathrm{A}_1 \cos[\omega_{\mathrm{dud}}(t-t_i)] \\ \qquad + \mathrm{A}_2 \sin[\omega_{\mathrm{dud}}(t-t_i)]\} \\ v_{\mathrm{np}}(t) = -a_{\mathrm{ud}} e^{-a_{\mathrm{ud}}(t-t_i)}\{\mathrm{A}_1 \cos[\omega_{\mathrm{dud}}(t-t_i)] \\ \qquad + \mathrm{A}_2 \sin[\omega_{\mathrm{dud}}(t-t_i)]\} \\ \qquad + \omega_{\mathrm{dud}} e^{-a_{\mathrm{ud}}(t-t_i)}\{-\mathrm{A}_1 \sin[\omega_{\mathrm{dud}}(t-t_i)] \\ \qquad + \mathrm{A}_2 \cos[\omega_{\mathrm{dud}}(t-t_i)]\} \\ \mathrm{A}_1 = u'_{\mathrm{np}}(t_i) \\ \mathrm{A}_2 = \frac{v'_{\mathrm{np}}(t_i) + \xi_{\mathrm{ud}}\omega_{\mathrm{nud}} u'_{\mathrm{np}}(t_i)}{\omega_{\mathrm{dud}}} \\ u_{\mathrm{ut}}(t) = u_{\mathrm{np}}(t) + u_{\mathrm{hv}}(t) \\ v_{\mathrm{ut}}(t) = v_{\mathrm{np}}(t) + v_{\mathrm{hv}}(t) \end{cases} \tag{18}$$

The displacement, $u_{\mathrm{fm}}(t)$, and velocity, $v_{\mathrm{fm}}(t)$, of the free mass after t_i as functions of time can be calculated using (10), as in

$$\begin{cases} u_{\mathrm{fm}}(t) = u'_{\mathrm{np}}(t_i) + v'_{\mathrm{fm}}(t_i)(t-t_i) + \frac{1}{2}g(t-t_i)^2 \\ v_{\mathrm{fm}}(t) = v'_{\mathrm{fm}}(t_i) + g(t-t_i) \end{cases} \tag{19}$$

B. COLLISION BETWEEN THE FREE MASS AND THE DRILL TOOL

The energy balance method is utilized to analyze the collision process of the free mass and the drill tool during rock drilling. The drill tool is a staircase structure, as shown in Fig. 7(a), and is regarded as a spring consisting of two springs with different spring rates, as shown in Fig. 7(b). The spring rates, k_{dt1} and k_{dt2}, are given by

$$\begin{cases} k_{\mathrm{dt1}} = \dfrac{E_{\mathrm{dt}} A_{\mathrm{dt1}}}{L_{\mathrm{dt1}}} \\ k_{\mathrm{dt2}} = \dfrac{E_{\mathrm{dt}} A_{\mathrm{dt2}}}{L_{\mathrm{dt2}}} \end{cases} \tag{20}$$

where E_{dt} is the elastic modulus of the drill tool, L_{dt1} and A_{dt1} are the length and cross-sectional area of part I of the drill tool respectively, and L_{dt2} and A_{dt2} are the length and cross-sectional area of part II of the drill tool respectively.

Assume that the drill tool and the free mass acquire the same velocity and move together immediately after impact

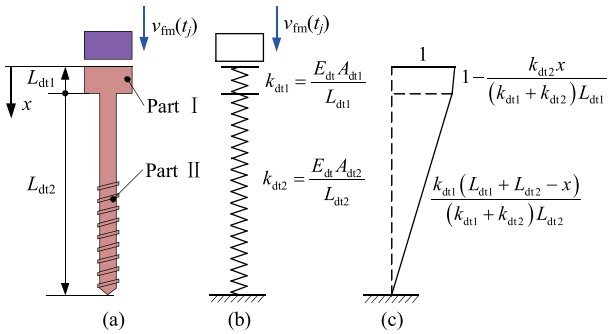

FIGURE 7. Collision model of the free mass and the drill tool during rock drilling. (a) The free mass impacting the drill tool. (b) The equivalent spring system. (c) The axial mode shape of the drill tool.

begins. Then, according to the law of conservation of momentum, the velocity of the free mass, $v'_{fm}(t_j)$, and the drill tool, $v'_{dt}(t_j)$, after t_j when the free mass and the drill tool produce the jth collision are given by

$$v'_{fm}(t_j) = v'_{dt}(t_j) = \frac{m_{fm}v_{fm}(t_j)}{m_{fm} + m_{eff,dt}} \tag{21}$$

where $m_{eff,dt}$ is the effective mass of the drill tool and is given by

$$m_{eff,dt} = \frac{\left(k_{dt1}^2 + 3k_{dt1}k_{dt1} + 3k_{dt2}^2\right)m_{dt1} + k_{dt1}^2 m_{dt2}}{3(k_{dt1} + k_{dt2})^2} \tag{22}$$

where $k_{dt1} = E_{dt}A_{dt1}/L_{dt1}$ is the spring rate of part I of the drill tool; $k_{dt2} = E_{dt}A_{dt2}/L_{dt2}$ is the spring rate of part II, as shown in Fig. 7(b); m_{dt1} is the mass of part I; and m_{dt2} is the mass of part II.

The axial deformation of the drill tool, $u_{dt}(x, t)$, is assumed to be of the form

$$u_{dt}(x, t) = \eta(t) f(x) \tag{23}$$

where $\eta(t)$ is the generalized dynamic axial deformation and $f(x)$ is the axial mode shape. As mentioned above, the drill tool is regarded as a spring consisting of two springs with different spring rates. The axial mode shape of the drill tool consists of two parts, as shown in Fig. 7(c). The mode shape, $f(x)$, is given by

$$f(x) = \begin{cases} 1 - \dfrac{k_{dt1}x}{(k_{dt1} + k_{dt2})L_{dt1}}, & 0 \leqslant x \leqslant L_{dt1} \\ \dfrac{k_{dt2}(L_{dt} - x)}{(k_{dt1} + k_{dt2})L_{dt2}}, & L_{dt1} < x \leqslant L_{dt} \end{cases} \tag{24}$$

where $L_{dt} = L_{dt1} + L_{dt2}$ is the total length of the drill tool.

The total kinetic energy of the drill tool, T_{dt}, is given by

$$T_{dt} = \frac{1}{2}\rho_{dt}A_{dt1}\int_0^{L_{dt1}}\left(\frac{\partial u_{dt}}{\partial t}\right)^2 dx + \frac{1}{2}\rho_{dt}A_{dt2}\int_{L_{dt1}}^{L_{dt}}\left(\frac{\partial u_{dt}}{\partial t}\right)^2 dx \tag{25}$$

where ρ_{dt} is the density of the drill tool.

Furthermore, the strain energy of the drill tool, V_{dt}, is given by

$$V_{dt} = \int_0^{L_{dt1}} \frac{A_{dt1}E_{dt}}{2}\varepsilon_{dt1}^2 dx + \int_{L_{dt1}}^{L_{dt}} \frac{A_{dt2}E_{dt}}{2}\varepsilon_{dt2}^2 dx \tag{26}$$

where $k_{eff,dt}$ is the effective spring rate of the drill tool and is given by

$$k_{eff,dt} = \frac{k_{dt1}^2 - k_{dt1}k_{dt2} + k_{dt2}^2}{k_{dt1} + k_{dt2}} \tag{27}$$

The Lagrange equation of the drill tool is given by

$$\frac{d}{dt}\left(\frac{\partial T_{dt}}{\partial \dot{\eta}}\right) - \frac{\partial T_{dt}}{\partial \eta} + \frac{\partial V_{dt}}{\partial \eta} = F_{cf} \tag{28}$$

where F_{cf} is the contact force between the free and the drill tool. The contact force can be calculated by substituting (25) and (26) into (27). Then, the contact force is given by

$$F_{cf} = m_{eff,dt}\ddot{\eta} + k_{eff,dt}\eta \tag{29}$$

The equation of motion for the free mass is given by

$$m_{fm}g - F_{cf} = m_{fm}\ddot{\eta} \tag{30}$$

The equation of motion for the system composed of the free mass and the drill tool can be obtained by combining (29) and (30), as in

$$\left(m_{fm} + m_{eff,dt}\right)\ddot{\eta} + k_{eff,dt}\eta = m_{fm}g \tag{31}$$

or

$$\ddot{\eta} + \omega_{fmdt}^2\eta = \frac{m_{fm}g}{m_{fm} + m_{eff,dt}} \tag{32}$$

where $\omega_{fmdt} = \sqrt{k_{eff,dt}/\left(m_{fm} + m_{eff,dt}\right)}$ is the natural frequency of the system. The solution of (32) is given by

$$\eta = A_3\sin(\omega_{fmdt}t) + B_3\cos(\omega_{fmdt}t) + \frac{m_{fm}g}{m_{fmdt}\omega_{fmdt}^2} \tag{33}$$

where A_3 and B_3 are undetermined coefficients, and $m_{fmdt} = m_{fm} + m_{eff,dt}$ is the mass of the system. A_3 and B_3 can be obtained using the initial conditions

$$\begin{cases} u_{dt}(x, 0) = u'_{dt}(t_j) \\ \dot{u}_{dt}(x, 0) = v'_{dt}(t_j) \end{cases} \tag{34}$$

Substituting the initial conditions, (34), into (33), A_3 and B_3 are given by

$$\begin{cases} A_3 = \dfrac{v'_{dt}(t_j)}{\omega_{fmdt}} \\ B_3 = u'_{dt}(t_j) - \dfrac{m_{fm}g}{m_{fmdt}\omega_{fmdt}^2} \end{cases} \tag{35}$$

Finally, η and $\ddot{\eta}$ are given by

$$\begin{cases} \eta = \dfrac{m_{fm}g}{m_{mfdt}\omega_{fmdt}^2} + \dfrac{v'_{dt}(t_j)}{\omega_{fmdt}}\sin\left[\omega_{fmdt}(t - t_j)\right] \\ \qquad + \left[u'_{dt}(t_j) - \dfrac{m_{fm}g}{m_{fmdt}\omega_{fmdt}^2}\right]\cos\left[\omega_{fmdt}(t - t_j)\right] \\ \ddot{\eta} = -\omega_{fmdt}v'_{dt}(t_j)\sin\left[\omega_{fmdt}(t - t_j)\right] \\ \qquad - \left[\omega_{fmdt}^2 u'_{dt}(t_j) - \dfrac{m_{fm}g}{m_{fmdt}}\right]\cos\left[\omega_{fmdt}(t - t_j)\right] \end{cases} \tag{36}$$

Then, the contact force, F_{cf}, can be calculated by substituting (36) into (28). The maximum contact force is obtained by differentiating (36) and equating it to zero, as in

$$\begin{cases} \dot{\eta} = \omega_{fmdt}\dfrac{v'_{dt}(t_j)}{\omega_{fmdt}}\cos\left[\omega_{fmdt}(t-t_j)\right] \\ \quad -\omega_{fmdt}\left[u'_{dt}(t_j)-\dfrac{m_{fm}g}{m_{fmdt}\omega_{fmdt}^2}\right]\sin\left[\omega_{fmdt}(t-t_j)\right] \\ \quad =0 \\ \ddot{\eta} = -\omega_{fmdt}^2 v'_{dt}(t_j)\cos\left[\omega_{fmdt}(t-t_j)\right] \\ \quad +\omega_{fmdt}\left[\omega_{fmdt}^2 u'_{dt}(t_j)-\dfrac{m_{fm}g}{m_{fmdt}}\right]\sin\left[\omega_{fmdt}(t-t_j)\right] \\ \quad =0 \end{cases} \tag{37}$$

By solving (37), the time t_{max} at which the compression and the acceleration reach their maximum values is given by

$$t_{max} = \frac{\arctan\left[\dfrac{\omega_{fmdt}m_{fmdt}v'_{dt}(t_j)}{\omega_{fmdt}^2 m_{fmdt}u'_{dt}(t_j)-m_{fm}g}\right]}{\omega_{fmdt}} + t_j \tag{38}$$

Then the contact time, t_{con}, for each collision process is given by

$$t_{con} = 2(t_{max}-t_j) = \frac{2\arctan\left[\dfrac{\omega_{fmdt}m_{fmdt}v'_{dt}(t_j)}{\omega_{fmdt}^2 m_{fmdt}u'_{dt}(t_j)-m_{fm}g}\right]}{\omega_{fmdt}} \tag{39}$$

C. SIMULATION AND DISCUSSION

A computer code is also employed to analyse the collision model of the percussive system during rock drilling. The initial parameters of the collision system are given in Table 2. The position of each component over time is shown in Fig. 8. The free mass oscillates between the actuator and the drill tool and impacts the drill tool approximately 282 times in 0.6 seconds, meaning that the impact frequency of the drill tool is nearly 470 Hz which is approximately equal to the impact frequency before drilling (430 Hz). Furthermore, the displacement of the upper side of the drill tool is only a few tens of microns, which is difficult to recognize in Fig. 8. Hence, a local zoomed in image of Fig. 8 is shown in Fig. 9.

TABLE 2. Simulation parameters for the percussive system during rock drilling.

Simulation parameter	Value
Mass of the RPUD m_{ud}	1000 g
Frequency of harmonic vibration f_0	16000 Hz
Amplitude of harmonic vibration A_0	35 μm
Damping ratio of the RPUD ξ_{ud}	0.5
Spring rate of the load spring k_1	2000 N/m
Mass of the free mass m_{fm}	5 g
Coefficient of restitution e_1	1
Elastic modulus of the drill tool E_{dt}	1.96×10^9 Pa
Length of part I of the drill tool L_{dt1}	10 mm
Cross sectional area of part I of the drill tool A_{dt1}	7.8×10^{-5} m^3
Length of part II of the drill tool L_{dt2}	80 mm
Cross sectional area of part II of the drill tool A_{dt2}	2.0×10^{-5} m^3
Density of the drill tool ρ_{dt}	7.9×10^3 kg/m^3

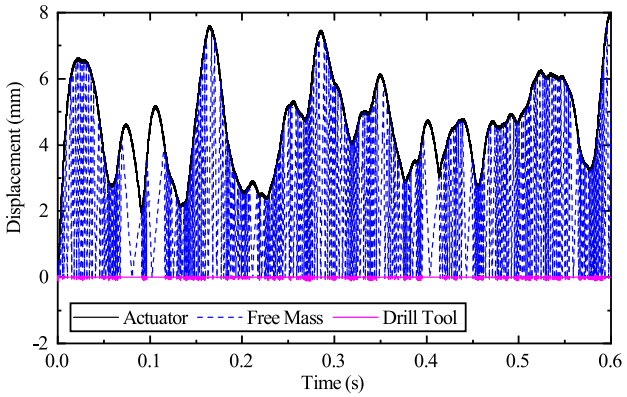

FIGURE 8. Positions of the actuator, the free mass and the drill tool as a function of time during rock drilling.

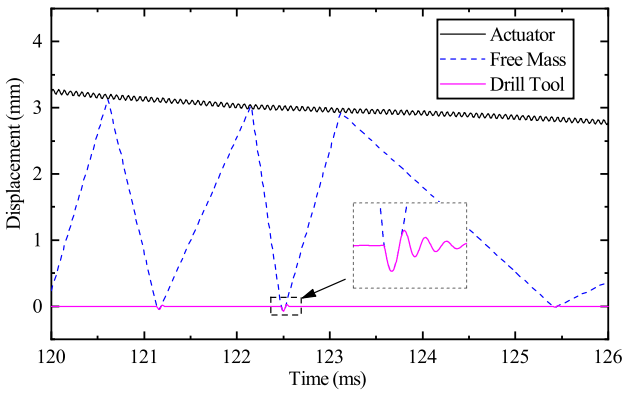

FIGURE 9. Local zoomed in image of Fig. 8 showing positions of the actuator, the free mass and the drill tool as functions of time.

The image shows that the end tip of the actuator experiences several cycles for each oscillation cycle of the free mass.

The maximum contact force between the free mass and the drill tool in each collision as a function of time is shown in Fig. 10. The image indicates that the maximum transient contact force reaches approximately 2600 N. Fig. 11 shows the distribution of the contact force in 0.6 seconds. It is observed that most of the contact forces are distributed in the range from 400N to 2200N. The collision process of the free mass and the drill tool is analyzed using the simulation parameters shown in Table 2. The initial velocity of the free mass is 5 m/s. Fig. 12 shows the displacement of the upper surface of the drill tool and the contact force versus time. The figure indicates that when impacted by a 5 g weight free mass with a velocity of 5 m/s, the maximum contact force between the free mass and the drill tool reaches 1650 N and the maximum displacement is 42 μm. The kinetic energy transferred to the drill tool as a function of time in 0.6 seconds is shown in Fig. 13. The figure indicates that the kinetic energy transferred to the drill tool in 0.6 seconds reaches 12.4 J. The reacting force represents the influence of the RPUD on the probe. Fig. 14 shows the reacting force as a function of time. The figure indicates that the reacting force fluctuates and the average value of the reacting force is 14 N.

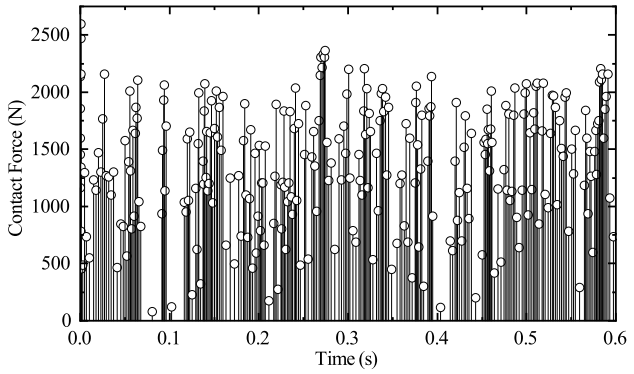

FIGURE 10. Maximum contact force between the free and the drill tool in each collision as a function of time.

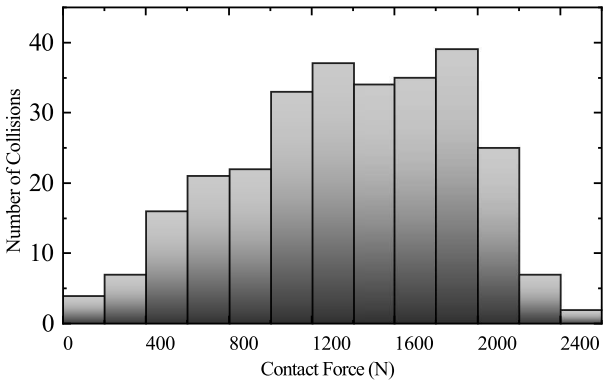

FIGURE 11. Distribution of the maximum contact force.

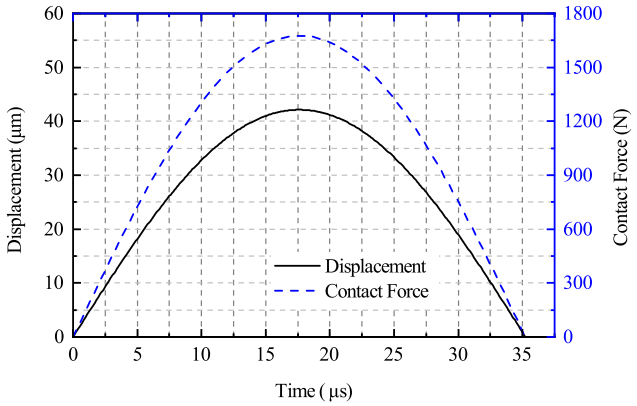

FIGURE 12. Displacement and contact force as functions of time during collision.

The effects of the coefficient of restitution e_1 on the average contact force, the number of collisions per second, the kinetic energy transferred to the drill tool per second, and the average reacting force were analysed. It can be seen that as the coefficient of restitution e_1 increases, the average contact force increases significantly, as shown in Fig. 15(a). Fig. 15(b) indicates an increasing coefficient of restitution e_1 results in a decrease in the number of collisions per second. The kinetic energy transferred to the drill tool per second

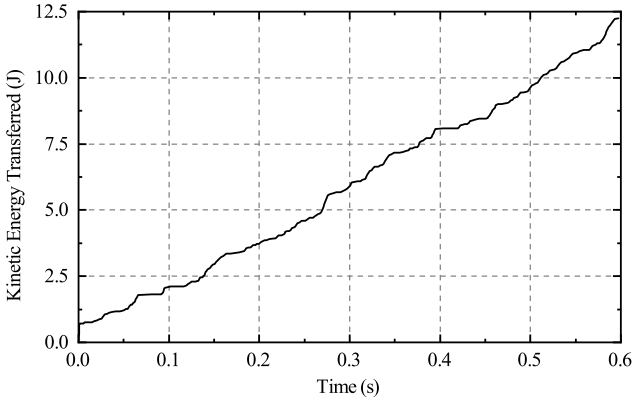

FIGURE 13. The kinetic energy transferred to the drill tool as a function of time.

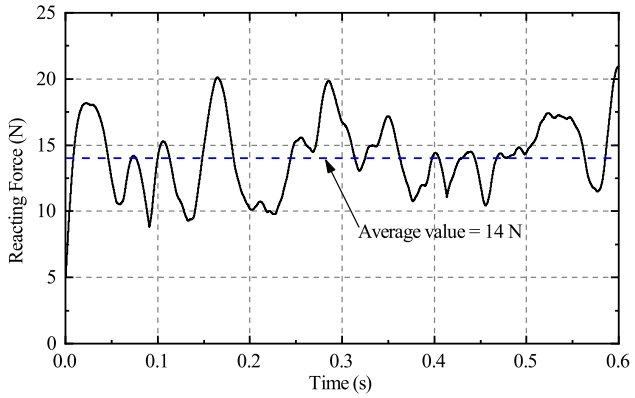

FIGURE 14. Reacting force acting on the load unit versus time during rock drilling.

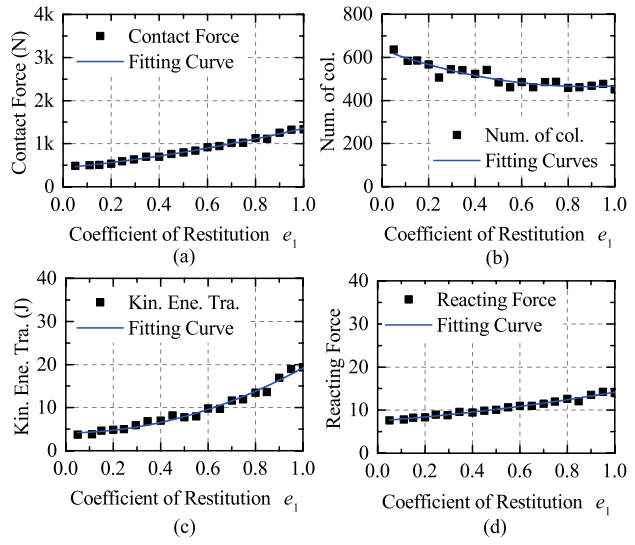

FIGURE 15. Effects of the coefficient of restitution e_1 on the percussive system. (a) The average contact force. (b) The number of collisions per second. (c) The kinetic energy transferred to the drill tool per second. (d) The reacting force.

and reacting force increase with an increasing coefficient of restitution e_1, as shown in Fig. 15(c) and Fig. 15(d).

The effects of the free mass on the average contact force, the number of collisions per second, the kinetic energy

transferred to the drill tool per second, and the average reacting force were analyzed, as shown in Fig. 16. The figure indicates that an increasing mass of the free mass results in an increase in the contact force, the kinetic energy transferred to the drill tool, and reacting force, as shown in Fig. 16(a), (c), and (d). Furthermore, number of collisions per second versus the weight of the free mass is shown in Fig. 16(b). The figure indicates that the number of collisions per second decreases with increasing free mass.

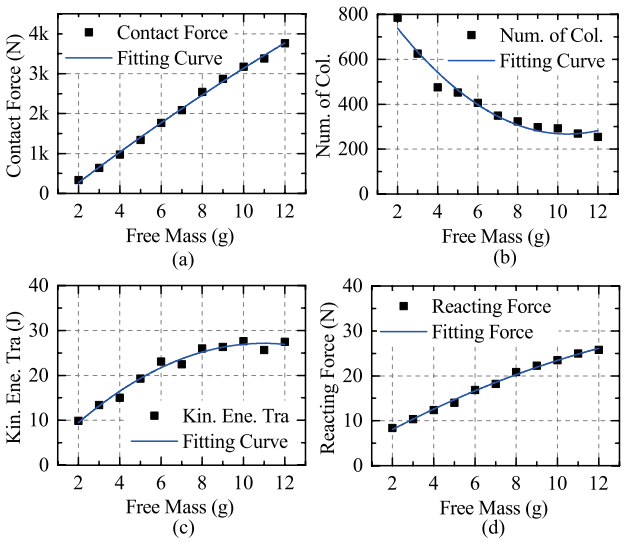

FIGURE 16. Effects of the free mass on the percussive system. (a) The average contact force. (b) The number of collisions per second. (c) The kinetic energy transferred to the drill tool per second. (d) The reacting force.

As mentioned above, the movement of the RPUD is modeled as a SDOF system after collision with the free mass. The damping ratio of the SDOF system ξ_{ud} was analysed, as shown in Fig. 17. The figure shows that changing ξ_{ud} has little effect on the contact force, as shown in Fig. 17(a). The number of collisions per second and the kinetic energy transferred to the drill tool per second increase with increasing ξ_{ud}, as shown in Fig. 17(b) and Fig. 17(d). Furthermore, the increase in ξ_{ud} leads to a decrease in the average reacting force, as shown in Fig. 17(c).

The weight on bit is an important control parameter for the RPUD during rock drilling. Fig. 18 shows simulation results of the weight on bit. It is observed that the changing of the weight on bit has little effect on the contact force, as shown in Fig. 18(a). Furthermore, the number of collisions per second, the kinetic energy transferred to the drill tool per second, and the reacting force increase with increasing weight on bit, as shown in Fig. 18(b), (c), and (d).

V. EXPERIMENTS

To verify the accuracy of calculation and simulation, several experiments are carried out. According to the calculation and simulation results presented in Section III, the displacement of the bottom side of the actuator consisted of the motion of the nodal plane and the harmonic vibration excited by the

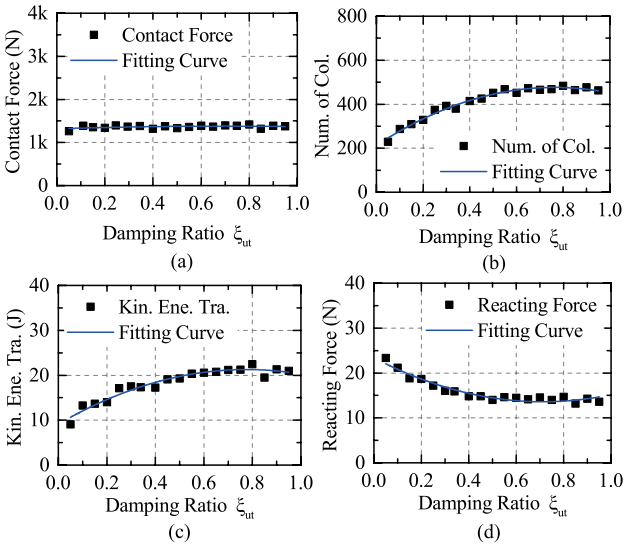

FIGURE 17. Effects of the damping ratio ξ_{ud} on the percussive system. (a) The average contact force. (b) The number of collisions per second. (c) The kinetic energy transferred to the drill tool per second. (d) The reacting force.

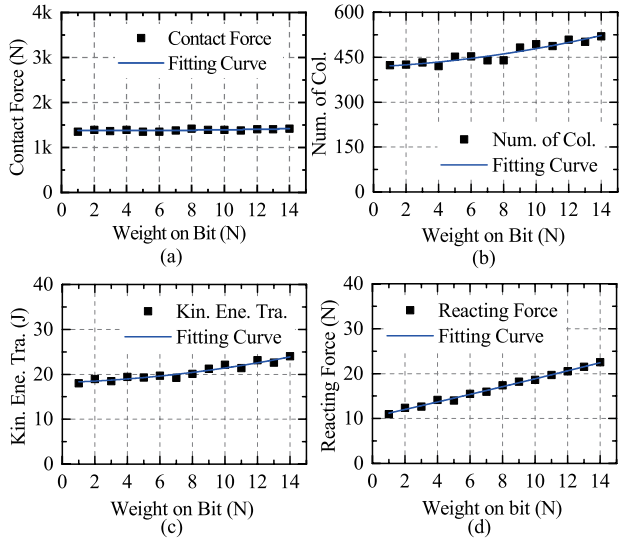

FIGURE 18. Effects of the weight on bit on the percussive system. (a) The average contact force. (b) The number of collisions per second. (c) The kinetic energy transferred to the drill tool per second. (d) The reacting force.

sinusoidal voltage. In addition, the displacement amplitude of the nodal plane is much bigger than that of the harmonic vibration. Hence, the harmonic vibration is ignored and the displacement of the nodal plane is regarded as the displacement of the bottom side of the actuator. The measurement method and a measurement system for the displacements and reacting force measurement of the percussive system are shown in Fig. 19. Two laser displacement sensors, LDS I and LDS II, are utilized to measure vibration displacements of the nodal plane and the drill tool, separately. Furthermore, the reacting force is measured by a load cell which is connected with the end of the load spring. Experimental results

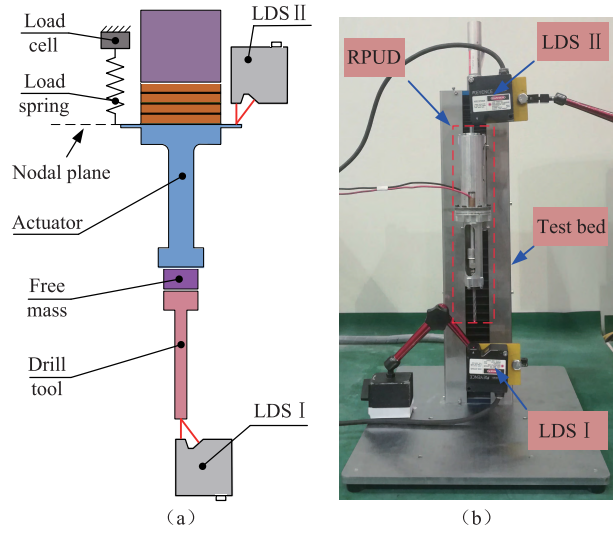

FIGURE 19. Displacements and reacting force measurement before rock drilling. (a) The measurement method. (b) The measurement system.

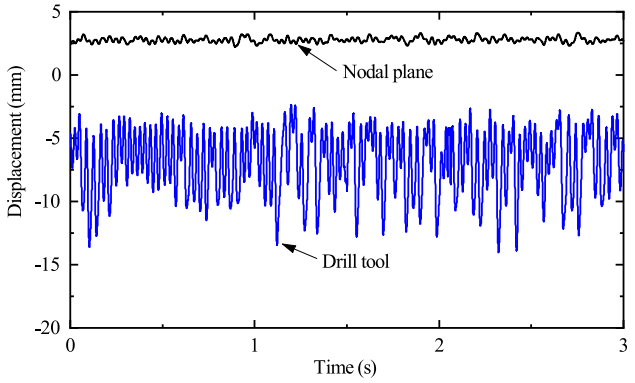

FIGURE 20. Experimental displacements of the nodal plane and the drill tool before rock drilling.

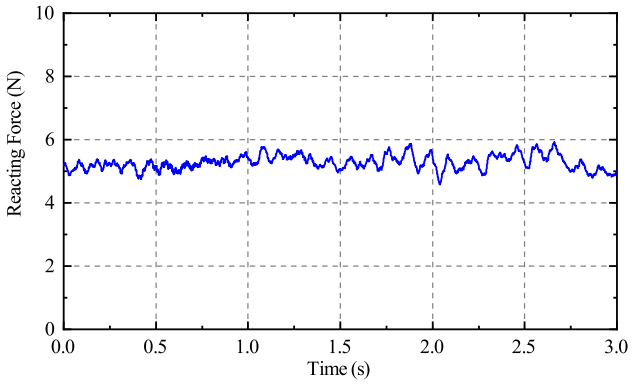

FIGURE 21. Experimental reacting force acting on the load unit versus time before rock drilling.

are shown in Fig. 20 and Fig. 21. The displacement amplitudes of the nodal plane and the drill tool during rock drilling are 2.6 mm and 14 mm respectively. Furthermore, the average reacting force is 5.2 N. The discrepancies between the simulation results and the experimental results are caused by the

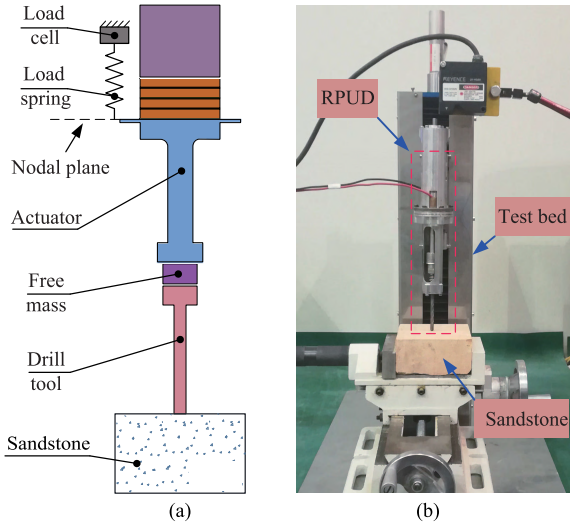

FIGURE 22. Reacting force measurement during rock drilling. (a) The measurement method. (b) The measurement system.

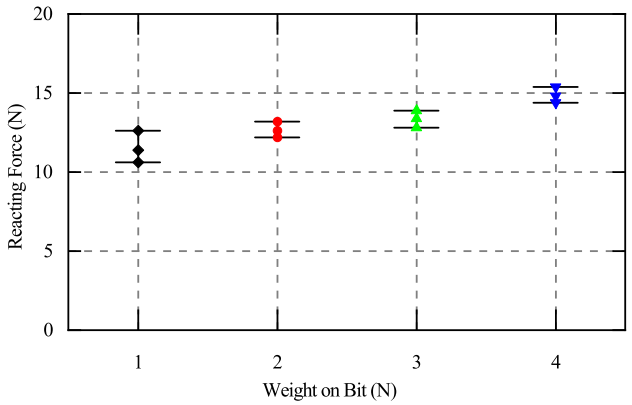

FIGURE 23. Experimental effects of the weight on bit on the reacting force.

differences between the simulation parameters and the real parameters of the RPUD during rock drilling.

Effects of the weight on bit on the reacting force is tested. The drill tool is pressed on a piece of sandstone with a mass density of 2360 kg/m^3, a compression strength of 75 MPa, and a Shore hardness of 31.9. Different weight on bits are applied on the RPUD and the corresponding reacting forces are measured by a load cell, as shown in Fig. 22. The reacting forces under different weight on bits are shown in Fig. 23. It indicates that the reacting force increase with increasing the weight on bit, which is consistent with the simulation result which is shown in Fig. 18(d).

VI. CONCLUSION

In this study, an impact dynamics prediction of a rotary-percussive ultrasonic drill including a free mass is presented. The interactions between the actuator, the free mass, and the drill tool before and during rock drilling were modeled, simulated, and discussed taking into consideration the vibration of

the RPUD and the weight on bit. Simulation results show that the increases in the coefficient of restitution e_1, the weight of the free mass, and the weight on bit cause increases in the contact force, kinetic energy transferred to the drill tool per second, and reacting force. In addition, increasing the damping ratio of the RPUD contributes to increases in both the contact force and the kinetic energy transferred to the drill tool per second and a decrease in the reacting force. Several experiments was carried out to verify the accuracy of calculation and simulation. The experimental results are consistent with the simulation results.

REFERENCES

[1] L. J. Vila and R. B. Malla, "Analytical model of the contact interaction between the components of a special percussive mechanism for planetary exploration," *Acta Astronaut.*, vol. 118, pp. 158–167, Jan./Feb. 2016.
[2] K. Zacny *et al.*, "Drilling systems for extraterrestrial subsurface exploration," *Astrobiology*, vol. 8, no. 3, pp. 665–706, Jun. 2008.
[3] Q. Quan, C. Chen, Z. Deng, J. Tang, and S. Jiang, "Recovery rate prediction in lunar regolith simulant drilling," *Acta Astronaut.*, vol. 133, pp. 121–127, Apr. 2017.
[4] X. Bao *et al.*, "Modeling and computer simulation of ultrasonic/sonic driller/corer (USDC)," *IEEE Trans. Ultrason., Ferroelectr., Freq. Control*, vol. 50, no. 9, pp. 1147–1160, Sep. 2003.
[5] P. Harkness and M. Lucas, "A brief overview of space applications for ultrasonics," *Ultrasonics*, vol. 52, no. 8, pp. 975–979, Dec. 2012.
[6] P. Harkness, M. Lucas, and A. Cardoni, "Coupling and degenerating modes in longitudinal–torsional step horns," *Ultrasonics*, vol. 52, no. 8, pp. 980–988, Dec. 2012.
[7] P. Harkness, M. Lucas, and A. Cardoni, "Architectures for ultrasonic planetary sample retrieval tools," *Ultrasonics*, vol. 51, no. 8, pp. 1026–1035, Dec. 2011.
[8] P. Harkness, M. Lucas, and A. Cardoni, "Maximization of the effective impulse delivered by a high-frequency/low-frequency planetary drill tool," *IEEE Trans. Ultrason., Ferroelectr., Freq. Control*, vol. 58, no. 11, pp. 2387–2396, Nov. 2011.
[9] C. Potthast, J. Twiefel, and J. Wallaschek, "Modelling approaches for an ultrasonic percussion drill," *J. Sound Vib.*, vol. 308, nos. 3–5, pp. 405–417, Dec. 2007.
[10] X. Li, P. Harkness, K. Worrall, R. Timoney, and M. Lucas, "A parametric study for the design of an optimized ultrasonic percussive planetary drill tool," *IEEE Trans. Ultrason., Ferroelectr., Freq. Control*, vol. 64, no. 3, pp. 577–589, Mar. 2017.
[11] L. J. Vila and R. B. Malla, "Dynamic impact force on a special drilling mechanism for planetary exploration," *J. Eng. Mech.*, vol. 29, no. 4, pp. 04016017-1–04016017-10, Jul. 2016.
[12] Y. Liu, X. Yang, W. Chen, and D. Xu, "A bonded-type piezoelectric actuator using the first and second bending vibration modes," *IEEE Trans. Ind. Electron.*, vol. 63, no. 3, pp. 1676–1683, Mar. 2016.
[13] G. Wang and Q. Xu, "Design and precision position/force control of a piezo-driven microinjection system," *IEEE/ASME Trans. Mechatronics*, vol. 22, no. 4, pp. 1744–1754, Aug. 2017.
[14] X. Yang, Y. Liu, W. Chen, and J. Liu, "Sandwich-type multi-degree-of-freedom ultrasonic motor with hybrid excitation," *IEEE Access*, vol. 4, pp. 905–913, Mar. 2016.
[15] J. Li *et al.*, "Development of a novel parasitic-type piezoelectric actuator," *IEEE/ASME Trans. Mechatronics*, vol. 22, no. 1, pp. 541–550, Feb. 2017.
[16] S. Park and S. He, "Standing wave brass-PZT square tubular ultrasonic motor," *Ultrasonics*, vol. 52, no. 7, pp. 880–889, 2012.
[17] D. Xu, Y. Liu, J. Liu, and W. Chen, "A bonded type ultrasonic motor using the bending of a crossbeam," *IEEE Access*, vol. 4, pp. 1109–1116, Mar. 2016.
[18] J. Shi and B. Liu, "Optimum efficiency control of traveling-wave ultrasonic motor system," *IEEE Trans. Ind. Electron.*, vol. 58, no. 10, pp. 4822–4829, Oct. 2011.
[19] T. Mashimo, "Scaling of piezoelectric ultrasonic motors at submillimeter range," *IEEE/ASME Trans. Mechatronics*, vol. 22, no. 3, pp. 1238–1246, Jul. 2017.
[20] P. A. Sente, F. M. Labrique, and P. J. Alexandre, "Efficient control of a piezoelectric linear actuator embedded into a servo-valve for aeronautic applications," *IEEE Trans. Ind. Electron.*, vol. 59, no. 4, pp. 1971–1979, Apr. 2012.
[21] X. Tang, Y. Liu, S. Shi, W. Chen, and X. Qi, "Development of a novel ultrasonic drill using longitudinal-bending hybrid mode," *IEEE Access*, vol. 5, pp. 7362–7370, Jun. 2017.
[22] K. Asumi, R. Fukunaga, T. Fujimura, and M. K. Kurosawa, "Miniaturization of a V-shape transducer ultrasonic motor," *Jpn. J. Appl. Phys.*, vol. 48, no. 7S, p. 07GM02, 2009.
[23] J.-T. Zhang, H. Zhu, S.-Q. Zhou, and C.-S. Zhao, "Optimal design of a rod shape ultrasonic motor using sequential quadratic programming and finite element method," *Finite Elements Anal. Des.*, vol. 59, no. 2, pp. 11–17, Oct. 2012.
[24] Y. Liu, S. Shi, C. Li, W. Chen, and J. Liu, "A novel standing wave linear piezoelectric actuator using the longitudinal-bending coupling mode," *Sens. Actuators A, Phys.*, vol. 251, pp. 119–125, Nov. 2016.
[25] Y. Liu, W. Chen, X. Yang, and J. Liu, "A rotary piezoelectric actuator using the third and fourth bending vibration modes," *IEEE Trans. Ind. Electron.*, vol. 61, no. 8, pp. 4366–4373, Aug. 2014.
[26] S. Sherrit, B. P. Dolgin, Y. Bar-Cohen, D. Pal, J. Kroh, and T. Peterson, "Modeling of horns for sonic/ultrasonic applications," in *Proc. IEEE Ultrason. Symp.*, vol. 1, Oct. 1999, pp. 647–651.
[27] S. Sherrit, M. Badescu, X. Bao, Y. Bar-Cohen, and Z. Chang, "Novel horn designs for power ultrasonics," in *Proc. IEEE Ultrason. Symp.*, vol. 3, Aug. 2004, pp. 2263–2266.
[28] L. J. Vila and R. B. Malla, "Elastoplastic contact force due to repeated longitudinal impacts on a novel percussive drill," *J. Eng. Mech.*, vol. 142, no. 10, pp. 04016075-1–04016075-10, Oct. 2016.
[29] Y. Wang, Q. Quan, H. Yu, H. Li, D. Bai, and Z. Deng, "Impact dynamics of a percussive system based on rotary-percussive ultrasonic drill," *Shock Vib.*, vol. 2017, no. 1, Oct. 2017. Art. no. 5161870.
[30] Y. Wang *et al.*, "A rotary-percussive ultrasonic drill for planetary rock sampling," in *Proc. IEEE/RSJ Int. Conf. Intell. Robots Syst.*, Daejeon, South Korea, Oct. 2016, pp. 2966–2971.

DEEN BAI was born in Shandong, China, in 1987. He received the B.S. degree in mechanical engineering from Northeast Forestry University, Harbin, China, in 2011, and the M.S. degree in mechanical engineering from the Harbin Institute of Technology, Harbin, in 2014, where he is currently pursuing the Ph.D. degree in mechanical engineering. His research interests include rotary-percussive ultrasonic drills and crushing efficiency for rock.

QIQUAN QUAN was born in Anhui, China, in 1983. He received the B.S. and M.S. degrees from the Harbin Institute of Technology, Harbin, China, in 2005 and 2007, respectively, and the Ph.D. degree from Ritsumeikan University, Japan. He is currently an Associate Professor with the State Key Laboratory of Robotics and System, Harbin Institute of Technology. His current research interests include in-orbit and on-ground testing of the aerospace mechanism.

YINCHAO WANG was born in Shandong, China, in 1985. He received the B.S. and M.S. degrees in mechanical engineering from Beihua University, China, in 2009 and 2012, respectively. He is currently pursuing the Ph.D. degree with the Harbin Institute of Technology, Harbin. His research interests are ultrasonic drilling sampling and piezoelectric actuation.

HE LI was born in Shandong, China, in 1987. He received the B.S. degree in mechanical engineering from the Changchun University of Science and Technology, Changchun, China, in 2010, and the M.S. degree in mechanical engineering from the Harbin Institute of Technology, Harbin, China, in 2013, where he is currently pursuing the Ph.D. degree in mechanical engineering. His research interests include ultrasonic levitating bearings.

PENGYUE ZHAO was born in Heilongjiang, China, in 1992. He received the B.S. and M.S. degrees in mechanical engineering from the Harbin Institute of Technology, Harbin, China, in 2014 and 2016, respectively, where he is currently pursuing the Ph.D. degree. His research interests include mars unmanned aerial vehicles and aerodynamics in low Reynolds number.

ZONGQUAN DENG was born in 1956. He received the B.S. and M.S. degrees from the Harbin Institute of Technology, Harbin, China, in 1982 and 1984, respectively. He is currently a Professor with the State Key Laboratory of Robotics and System, Harbin Institute of Technology. His current research interests include special robot systems and aerospace mechanisms and control.